



Geophysical Research Letters



RESEARCH LETTER

10.1029/2023GL107085

Key Points:

- We present observations of magnetopause erosion at geosynchronous orbit caused by reconnection
- Magnetopause erosion showed dawndusk asymmetry
- Asymmetric erosion can plausibly be attributed to a reduced reconnection rate at the duskside magnetopause due to cold dense plasma

Supporting Information:

Supporting Information may be found in the online version of this article.

Correspondence to:

H. Kim, holypyo@gmail.com; hyangpyo.kim@oeaw.ac.at

Citation:

Kim, H., Nakamura, R., Connor, H. K., Zou, Y., Plaschke, F., Grimmich, N., et al. (2024). Localized magnetopause erosion at geosynchronous orbit by reconnection. *Geophysical Research Letters*, 51, e2023GL107085. https://doi.org/10.1029/ 2023GL107085

Received 3 NOV 2023 Accepted 5 FEB 2024

Localized Magnetopause Erosion at Geosynchronous Orbit by Reconnection

Hyangpyo Kim¹, Rumi Nakamura¹, Hyunju K. Connor², Ying Zou³, Ferdinand Plaschke⁴, Niklas Grimmich⁴, Brian M. Walsh⁵, Kathryn A. McWilliams⁶, and J. Michael Ruohoniemi⁷

¹Space Research Institute, Austrian Academy of Sciences, Graz, Austria, ²NASA Goddard Space Flight Center, Greenbelt, MD, USA, ³Johns Hopkins University Applied Physics Laboratory, Laurel, MD, USA, ⁴Institute of Geophysics and Extraterrestrial Physics, Technische Universität Braunschweig, Braunschweig, Germany, ⁵Center for Space Physics, Boston University, Boston, MA, USA, ⁶Institute of Space and Atmospheric Studies, University of Saskatchewan, Saskatoon, SK, Canada, ⁷Bradley Department of Electrical and Computer Engineering, Virginia Tech, Blacksburg, VA, USA

Abstract This study presents observations of magnetopause reconnection and erosion at geosynchronous orbit, utilizing in situ satellite measurements and remote sensing ground-based instruments. During the main phase of a geomagnetic storm, Geostationary Operational Environmental Satellites (GOES) 15 was on the dawnside of the dayside magnetopause (10.6 MLT) and observed significant magnetopause erosion, while GOES 13, observing duskside (14.6 MLT), remained within the magnetosphere. Combined observations from the THEMIS satellites and Super Dual Auroral Radar Network radars verified that magnetopause erosion was primarily caused by reconnection. While various factors may contribute to asymmetric erosion, the observations suggest that the weak reconnection rate on the duskside can play a role in the formation of asymmetric magnetopause shape. This discrepancy in reconnection rate is associated with the presence of cold dense plasma on the duskside of the magnetosphere, which limits the reconnection rate by mass loading, resulting in more efficient magnetopause erosion on the dawnside.

Plain Language Summary The boundary of Earth's magnetosphere, knows as the magnetopause, moves back and forth in response to the upstream solar wind conditions, mainly solar wind dynamic pressure and the north-south component of the interplanetary magnetic field (IMF). It is well known that the magnetopause moves closer to the Earth during periods of southward IMF compared to northward IMF. This phenomenon occurs because reconnection between the IMF and Earth's magnetic field removes magnetic flux at the boundary layer, resulting in magnetopause erosion. Occasionally, the magnetopause approaches geosynchronous orbit when the magnetosphere is highly compressed and/or eroded, mainly during geomagnetic storms. Statistical studies have shown the magnetopause erosion often shows a dawn-dusk asymmetry at geosynchronous orbit. This study presents concurrent observations of magnetopause erosion and related dayside reconnection at geosynchronous orbit by utilizing data from THEMIS, Geostationary Operational Environmental Satellites, and Super Dual Auroral Radar Network radar. The observations suggest that the presence of cold dense plasma in the duskside magnetosphere weakens reconnection rates and, consequently, it contributed to the dawn-dusk asymmetry of magnetopause erosion.

1. Introduction

The magnetopause moves closer to Earth during periods of southward interplanetary magnetic field (IMF) compared to periods of northward IMF, because reconnection between the IMF and Earth's magnetic field removes magnetic flux from the dayside (e.g., Fairfield, 1971; Maezawa, 1974; Petrinec et al., 1991; Tsyganenko & Sibeck, 1994). Occasionally, the magnetopause reaches geosynchronous orbit (6.6 $R_{\rm E}$) when the magnetosphere undergoes significant compression and/or erosion (e.g., Russell, 1976). In an early study using Geostationary Operational Environmental Satellites (GOES) 2, 5, and 6 satellites, Rufenach et al. (1989) suggested that both high solar wind dynamic pressure and southward IMF are necessary for the excursion of the magnetopause to geosynchronous orbit. Dynamic pressure alone is inadequate; thus, some erosion is required. Recently, Le et al. (2016) reported a strong magnetopause erosion bring the boundary to the geosynchronous orbit during a

© 2024. The Authors.

This is an open access article under the terms of the Creative Commons

Attribution License, which permits use, distribution and reproduction in any medium, provided the original work is properly cited.

KIM ET AL. 1 of 11

geomagnetic storm. The study concluded that the erosion was primarily driven by dayside reconnection, supported by the intensification of field-aligned currents and polar cap expansion.

Statistical studies have shown that geosynchronous magnetopause crossings (GMC) are predominantly observed on the dawnside, showing dawn-dusk asymmetry, during extreme solar wind conditions (e.g., Dmitriev et al., 2004; Fairfield et al., 1990; McComas et al., 1993, 1994; Wrenn et al., 1981). Fairfield et al. (1990) suggested that pressure variations in the magnetosheath, associated with a foreshock, leads naturally to an increased chance of observing a crossing on the dawnside. McComas et al. (1993) showed magnetosheath preferentially encountered on the prenoon side and magnetopause shape is highly asymmetric about the Sun-Earth line. Dmitriev et al. (2004) analyzed 326 GMCs and found that asymmetry is more pronounced when the IMF is strongly southward, while the magnetopause shape tends to be symmetrical during periods of northward IMF. The work suggested that the primary cause of this asymmetry is the more intense magnetopause erosion in the prenoon sector and the strong asymmetry of the ring current, rather than solar wind aberration.

While many measurements of GMCs exist, previous studies have primarily relied on statistical analysis and have not directly explored the role of magnetic reconnection in magnetopause erosion. The current understanding of the causes of asymmetric magnetopause erosion remains incomplete. This gap is due to experimental limitations preventing simultaneous measurements of the outer magnetosphere at different local times. This letter presents the direct observations of magnetopause erosion and its related reconnection by utilizing in situ satellites and ground-based instruments.

2. Instrumentation

The current work utilized in situ measurements from the Time History of Events and Macroscale Interactions during Substorms (THEMIS) mission (Angelopoulos, 2008). The study used magnetic field measurements from the Fluxgate Magnetometer (FGM; Auster et al., 2008) and plasma moments such as ion bulk velocity, energy distribution, and density from Electrostatic Analyzer (ESA; McFadden et al., 2008). The electron density inferred from the spacecraft potential measured by the Electric Field Instrument (EFI; Bonnell et al., 2008) was also used. To identify instances of geosynchronous magnetopause erosion, the study used magnetic field measurements from the GOES, spacecraft orbiting at geosynchronous orbit around Earth (6.6 $R_{\rm F}$).

For investigating reconnection behavior, the study employed remote sensing utilizing the Super Dual Auroral Radar Network (SuperDARN), which measures Doppler-shifted ionospheric convection flows (Chisham et al., 2007; Greenwald et al., 1995; Nishitani et al., 2019). The study used data collected from specific Super-DARN sites: Prince George (PGR; 59.6° MLAT, -64.3° MLON), Saskatoon (SAS; 60.9° MLAT, -43.8° MLON), and Kapuskasing (KAP; 60.2° MLAT, -8.3° MLON), which observe the meridional plasma flows over the ionospheric footprints of geosynchronous orbit. The flow velocity vectors were obtained by merging line-of-sight measurements within the overlapping field of view of the radars (Ruohoniemi & Baker, 1998). To complement our analysis, the study incorporated measurements of Global Positioning System (GPS) total electron content (TEC).

3. Observations

Figure 1 presents an overview of the 27 February 2014 event. The locations of the satellites and a model estimation of the magnetopause are presented in Figures 1h and 1i. The top three panels (Figures 1a-1c) present the IMF, solar wind dynamic pressure (P_{sw}), and SYM-H index obtained from the OMNI data set. During a prolonged southward IMF period, strong pressure enhancements (12 and 17 nPa) and a SYM-H increase (20 nT) were observed after 16:50 UT, representing the sudden commencement phase of the geomagnetic storm. Then, SYM-H decreased and reached a minimum value of -100 nT at 23:25 UT (not shown here) indicating the period of storm main phase. During this period, THEMIS D (THD) was positioned near noon (>12.8 MLT) and at a distance of 11 $R_{\rm F}$ from the Earth.

Figures 1d and 1e present THD observations of the magnetic field and ion bulk velocity. A strong negative B_z and slow V_x before 16:50 UT indicate that THD was located in the magnetosheath. After the pressure enhancement, the magnetopause was compressed. The magnetopause model predicts the subsolar point to be compressed to a radial distance of 7 R_E . This relocation allows THD to probe the IMF and the upstream solar wind with a flow

KIM ET AL. 2 of 11

19448007, 2024, 5, Downloaded from https://agupubs.onlinelibrary.wiley.com/doi/10.1029/2023GL107085 by Boston University, Wiley Online Library on [02/05/2024]. See the Terms and Conditions (https://onlinelibrary.wiley.com/terms-and-conditions).

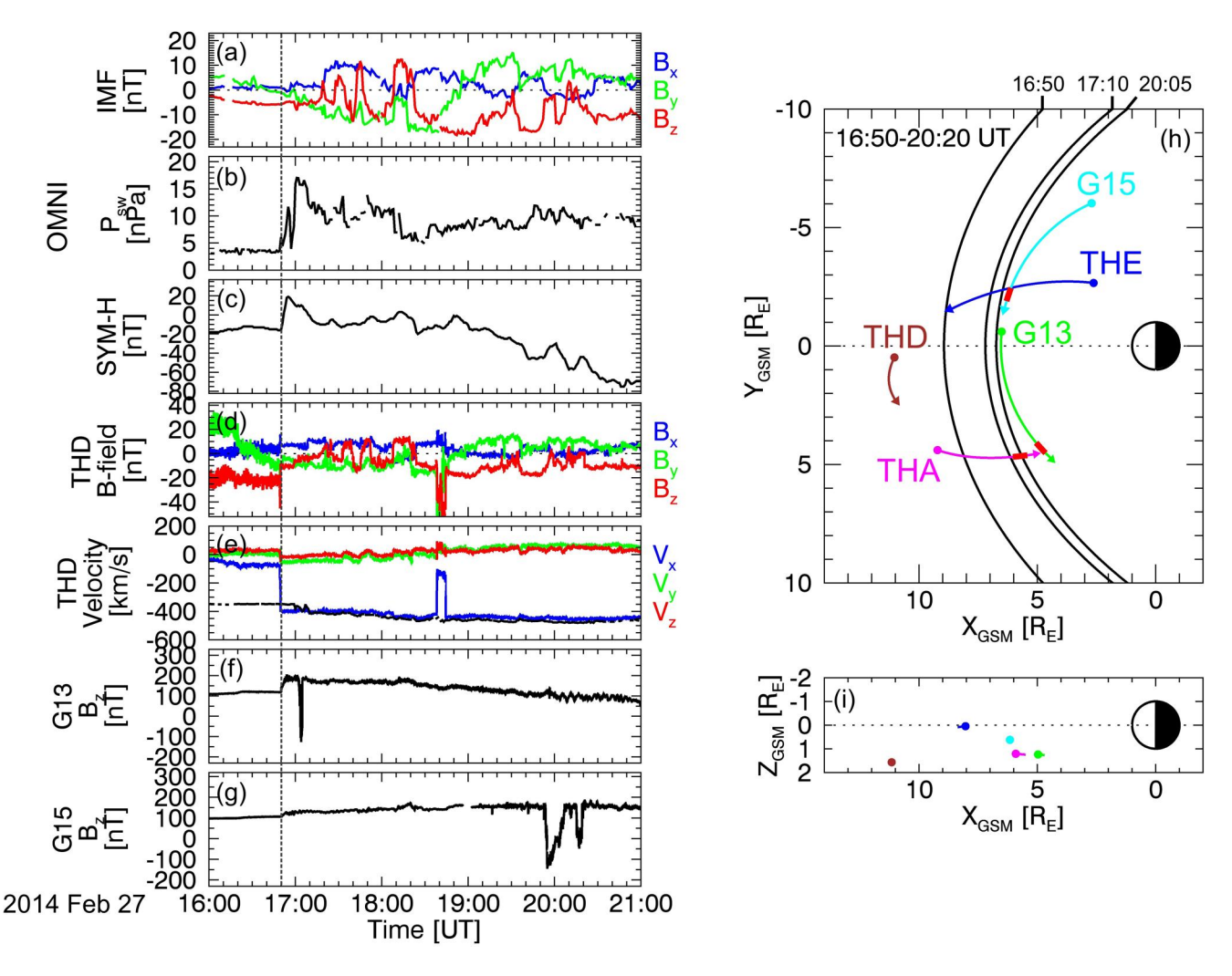


Figure 1. Overview of 27 February 2014 event. Left panels present OMNI (a) interplanetary magnetic field (IMF) in GSM coordinate, (b) solar wind dynamic pressure, and (c) SYM-H index. (d, e) THEMIS D measurements of magnetic field and ion flow velocity in GSM coordinate. (f, g) G13 and G15 measurements of B_z component of magnetic field. The black dashed line indicates the onset of pressure enhancement at 16:50 UT. Right: satellites orbits during 16:50–20:20 UT projected to the (h) GSM XY and (i) XZ planes. Black curves indicate magnetopause locations at 16:50 UT, 17:10 UT, and 20:05 UT using Shue et al. (1998) model. Five-minute averaged IMF and solar wind dynamic pressure were used as input parameters. Red thick lines mark a period of asymmetric geosynchronous magnetopause crossings during 19:52–20:07 UT.

velocity of $V_{\rm x} \approx -400$ km/s, which closely matched the OMNI solar wind velocity $V_{\rm x}$ (black line in Figure 1e). The magnetosheath temporarily expanded around 18:40 UT accompanied by significant decreases in $|V_{\rm x}|$ and B_z .

Figures 1f and 1g show the B_z component of magnetic field as measured by GOES 13 (G13) and GOES 15 (G15). During the event, G13 was primarily located in the dusk sector (11.6–15 MLT) while G15 was positioned in the dawn sector (7.6–11 MLT). Following a pressure enhancement at 16:50 UT, both satellites observed an increase in the B_z associated with the magnetopause current (Chapman & Ferraro, 1931); G13 recorded a larger increase, possibly because it was located near the subsolar magnetopause. The significant drop in B_z , that is, the GMC, was initially observed by G13 at 17:02 UT. This reduction in B_z can be chiefly attributed to the compression of the magnetopause, driven by a substantial pressure increase of 17 nPa. Following this observation, no further GMCs were observed on the duskside, despite variations in solar wind pressure ranging from 5 to 14 nPa. On the dawnside, G15 detected two transient GMCs at 19:52–20:07 UT and 20:15–20:20 UT (Figure 1g) while G13 remained within the magnetosphere, showing the dawn-dusk asymmetry of GMC. Note that the model estimation of the magnetopause indicated that magnetopause was closer to Earth at 20:05 UT when IMF B_z was -12.77 nT than at 17:10 UT when IMF B_z was -5.39 nT, even though the solar wind pressure was higher at 17:10 UT

KIM ET AL. 3 of 11

19448007, 2024, 5, Downloaded from https://agupubs.onlinelibrary.wiley.com/doi/10.1029/2023GL107085 by Boston University, Wiley Online Library on [02/05/2024]. See the Terms and Condition

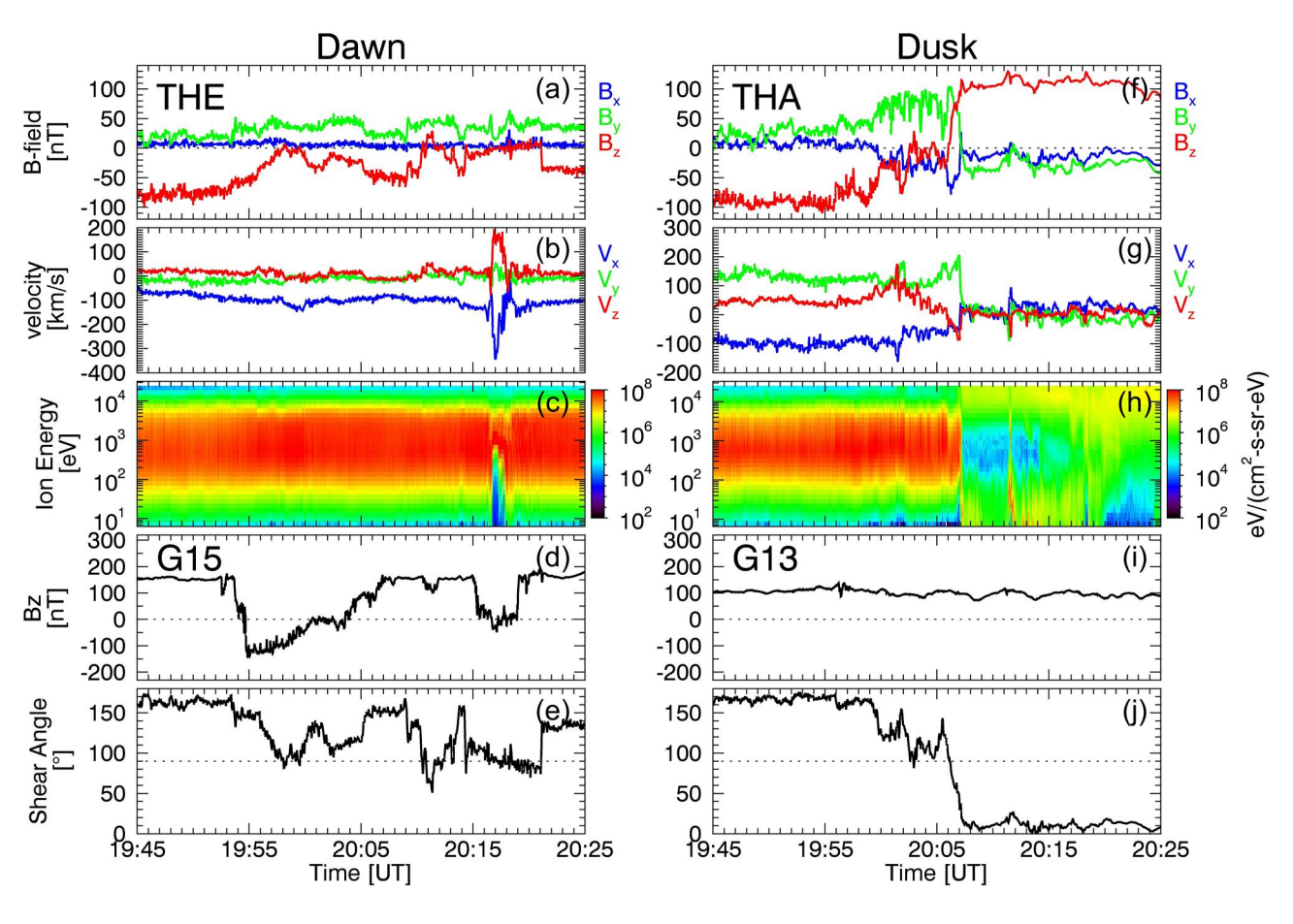


Figure 2. In situ observations during asymmetric magnetopause erosion. (a–c) THE measurements of magnetic field, ion flow velocity, and ion energy spectra. (d) B_z component of magnetic field measured by G15. (e) Magnetic shear angles between the magnetosheath and the magnetosphere. (f–j) Similar to panels (a–e) but showing measurements by THA and G13.

(14.3 nPa) than at 20:05 UT (9.45 nPa). This implies that reconnection contributed more to the magnetopause moving toward the Earth when G15 crossed the magnetopause.

Figure 2 presents measurements from THEMIS and GOES during a period between 19:45 and 20:25 UT. The MLT separation between THE and G15 was 0.3–0.6 hr during this window, while the separation between THA and G13 was 0.3 hr. THE was primarily in the dawnside magnetosheath, while THA spent an equal interval of time in both the duskside magnetosheath and the magnetosphere. In the dawn magnetosheath, the magnetic field remained predominantly southward throughout the interval, except for brief periods around 19:58 UT and 20:11 UT (Figure 2a). The magnetic field in the dusk sector was predominantly southward but its magnitude differed from the dawn sector (Figure 2f), possibly due to different magnetosheath conditions. In the magnetosheath, the ion bulk velocity ($V_x > -150 \, \text{km/s}$) was notably slower compared to the solar wind ($V_x < -400 \, \text{km/s}$) and the ion energy spectra exhibited a wide distribution (Figures 2b, 2c, 2g, and 2h). During the asymmetric GMC between 19:52 and 20:07 UT (Figures 2d and 2i), both THE and THA were in the magnetosheath and no remarkable changes were observed in either the dawn and dusk sectors. However, the GMC between 20:15 and 20:20 UT was most likely caused by local pressure enhancements in the dawnside, since THE was temporarily in the solar wind during that period (Figures 2b and 2c), that is, magnetosphere was strongly compressed.

Assuming minimal change in the magnetic field along the GOES orbit compared to the magnetic field at 19:50 UT (prior to GMC), the study estimated the shear angle of the magnetic field lines between the magnetosheath and the magnetosphere as shown in Figures 2e and 2j. The study used THEMIS measurements for the magnetosheath's magnetic field and GOES measurements at 19:50 UT for the magnetosphere's magnetic field. These shear angles varied over 140°–80°, indicating that component reconnection may have dominantly occurred on both sides (Trattner et al., 2021).

KIM ET AL. 4 of 11

19448007, 2024, 5, Downloaded from https://agupubs.onlinelibrary.wiley.com/doi/10.1029/2023GL 107085 by Boston University, Wiley Online Library on [02/05/2024]. See the Terms and Cond

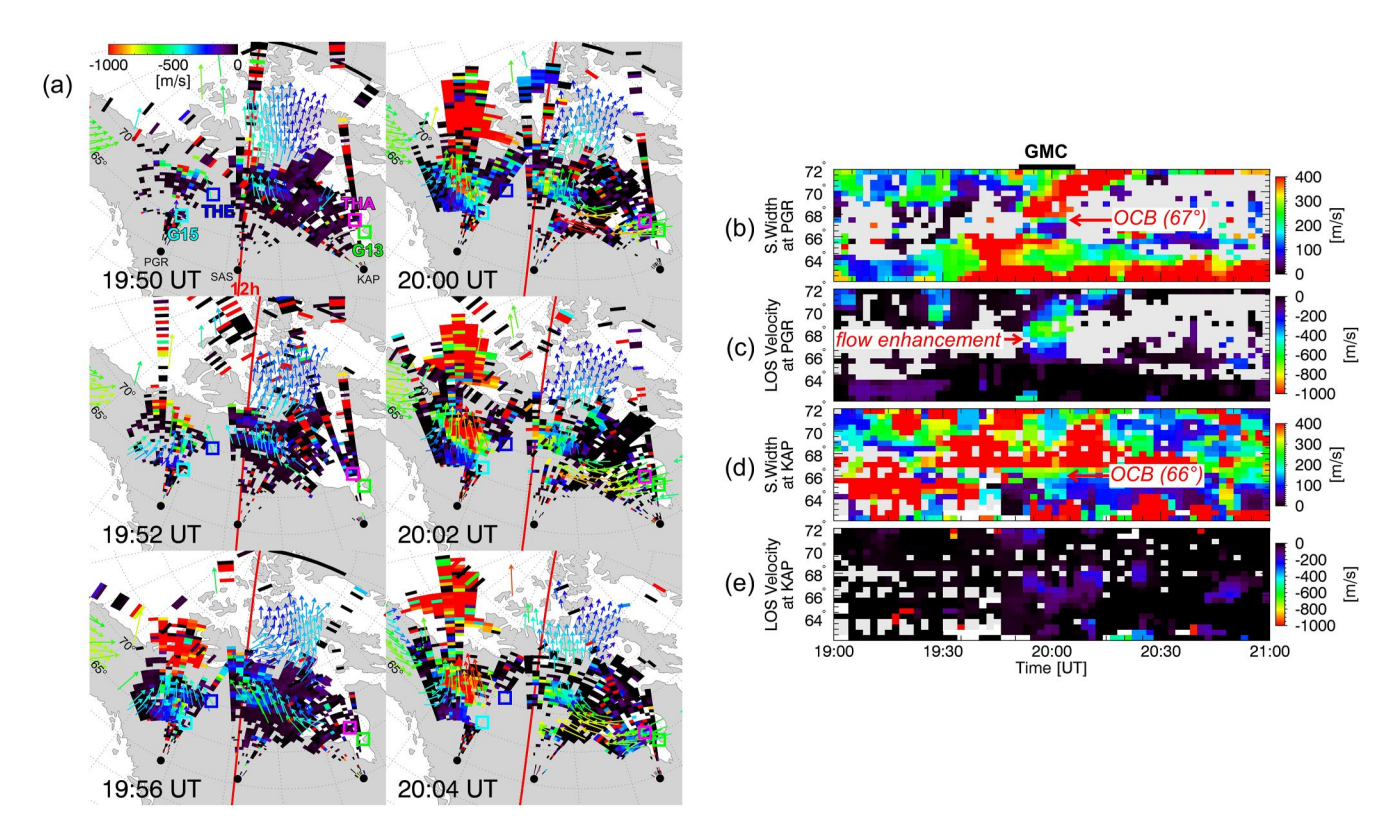


Figure 3. SuperDARN observations during asymmetric geosynchronous magnetopause crossings in AACGM coordinate. (a) Line-of-sight plasma velocity within the radar field of view. Arrows indicate merged velocity vectors inferred from multiple radars. (b) Temporal variations of spectral width and plasma velocity measured by PGR radar beam 11 and KAP radar beam 13, respectively. The gray colors indicate ground-scattered signals.

To investigate whether the magnetopause erosion was related to reconnection, Figure 3 presents SuperDARN observations in Altitude Adjusted Corrected Geomagnetic (AACGM) coordinates (Shepherd, 2014). The fast anti-sunward flow across the ionospheric projection of the reconnection separatrix, known as the open-closed boundary (OCB), has been a clear indicator of dayside reconnection. Figure 3a shows line-of-sight observations of plasma flow velocity within the radar field of view from 19:50 to 20:06 UT. The longer period plots from 16:50 to 20:20 UT are shown in Figure S1. The colored tiles represent velocities along the radar line-of-sight (poleward flow), while the black tiles indicate velocities directed opposite to the line-of-sight (equatorward flow). Velocity vectors are superimposed on a color scale ranging from 0 to 1,000 m/s. Satellite's footprints deduced from the TS04 magnetic field model (Tsyganenko & Sitnov, 2005) are marked by colored squares. Note that the study also utilized the T89 model (Tsyganenko, 1989) for THE since its footprint often extends into the solar wind when using TS04 model. Before 19:52 UT, strong poleward flows were predominantly observed at latitudes above 70° MLAT, while equatorward or weak poleward flows (>-50 km/s) dominated at footprints of the geosynchronous spacecraft (also refer to Figure S1). The strong poleward flows (-300 km/s) were first observed at 19:52 UT in the north-west direction from G15 footprint (66° MLAT). This velocity then increased to -600 km/s at 19:56 UT, with even higher velocities recorded above the G15 footprint, peaking at -1,000 km/s. These strong flows around G15 footprint persisted until 20:04 UT although radar echoes were sparse at a few points.

In the dusk sector, dawnward flows were predominantly observed around the G13 footprint in the ionosphere, showing typical two-cell convection pattern during southward IMF with positive B_y . The velocities at the footprint of G13 were considerably lower than those observed at G15. These observations suggest that reconnection predominantly/or effectively took place on dawnside and subsolar region during the asymmetric magnetopause erosion. Note that no remarkable poleward flows were detected during GMCs around 17:00 UT and 20:15 UT as shown in Figures S1a and S1c, supporting the idea that these GMCs were primarily caused by local pressure enhancements rather than reconnection.

KIM ET AL. 5 of 11

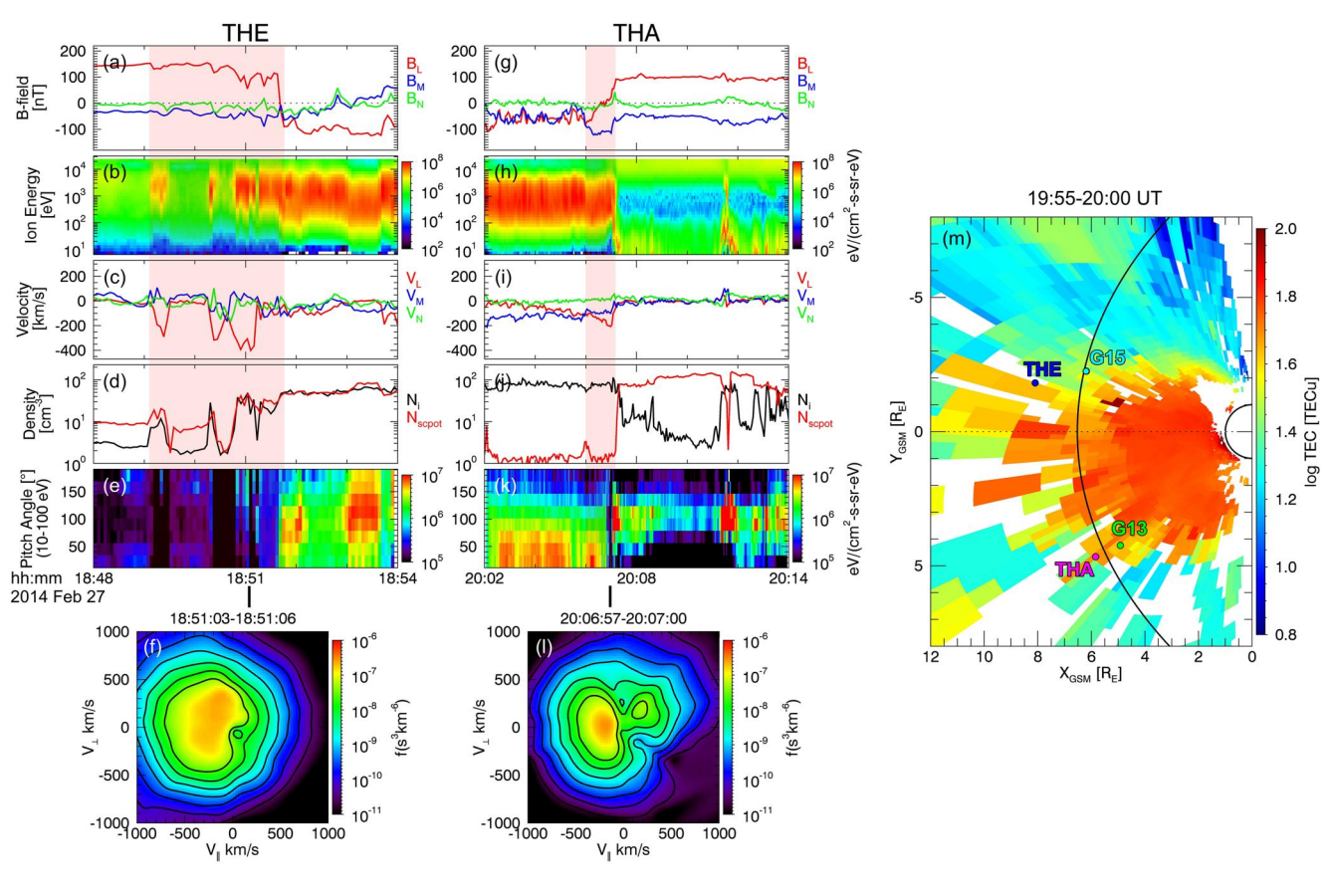


Figure 4. Observations of magnetopause crossings from THE and THA. (a, g) Magnetic field, (b, c) ion energy spectra, (c, f) ion flow velocity, and (d, j) ion density measured from ESA (black) and electron density inferred from spacecraft potential (red). The magnetic field and ion velocity are in boundary normal coordinates (LMN) determined through minimum variance analysis. Pink shades indicate the intervals of magnetopause crossing. (e, k) Pitch angle distribution of ion within the energy range of 10–100 eV. (f, l) Ion velocity distribution. (m) Global Positioning System total electron content measurements during 19:55–20:00 UT projected to the equatorial plane of the magnetosphere following magnetic field lines with the International Geomagnetic Reference Field model.

Using the assumption that the magnetic field lines are frozen into plasma that flows perpendicular to Earth's magnetic field, the study estimated the reconnection rate by measuring the magnetic flux transfer across the OCB, that is, the electric field along the OCB in the OCB moving reference frame: $E = (V_o - V_p) \times B$, where V_o and V_p are the velocity of OCB and plasma, and B is the magnetic field obtained from International Geomagnetic Reference Field (IGRF) model (e.g., Cowley & Lockwood, 1992; Hubert et al., 2006; Zou et al., 2019, 2021, 2022). The OCB can be inferred as the location of a distinct boundary in spectral width but the threshold can vary in individual events (e.g., Chen et al., 2016; Chisham & Freeman, 2003; Chisham et al., 2008; Zou et al., 2019, 2022). Figures 3b–3e show the temporal variations of spectral width and flow velocity as measured by beam 11 of PGR and beam 12 of KAP, respectively, with a 0.5° MLAT binning and a 2-min time resolution. The study selected these beams because they reveal a clear equatorward boundary in spectral width. To refine the data, we applied a 3×3 spatio-temporal median filter, following the method by Chisham and Freeman (2003), to eliminate any isolated or spurious peak echoes. The study defined the OCB as the region characterized by the largest gradient in spectral width within the area marked by strong poleward plasma flows. In this study, it corresponds to the boundaries of 200-350 m/s spectral widths. During an interval of asymmetric GMC, the OCBs were consistently positioned at approximately 67° MLAT in PGR and 66° MLAT in KAP. The average reconnection electric fields were calculated as 26.3 mV/m with a standard deviation of 2 mV/m for PGR and 5.8 mV/m with a standard deviation of 3. 2 mV/m for KAP, respectively. These values suggest stronger or more efficient reconnection near the G15 location.

Next, the study investigated reconnection behavior at the magnetopause. Figure 4 shows measurements from THE and THA in boundary normal coordinates (LMN), where L signifies the direction of outflow, M is along the X-line, and N corresponds to the current sheet normal. The determination of this coordinate system is based on the

KIM ET AL. 6 of 11

minimum variance analysis of the magnetic field (Sonnerup & Cahill, 1967) during 18:51:35–18:51:45 UT (20:02:00–20:12:00 UT) for THE (THA). Since THE was in the magnetosheath during the GMC, the study presents a THE outbound crossing of boundary in the interval from 18:48 to 18:54 UT. Note that during that period, SuperDARN observations generally indicated stronger poleward flows in the dawnside compared to the duskside (see Figure S1b). Therefore, while the magnetosheath/magnetosphere conditions in dawnside and duskside may differ during the period of asymmetric GMC, it would be useful to examine the reconnection rate in dawnside during this time period.

THE encountered the magnetopause several times between 18:49:10 and 18:51:40 UT (pink shaded, \sim 7.1 R_E from the Earth), detecting dense and fast-flowing plasma of the solar wind origin (Figures 4c and 4d). These magnetopause encounters indicate that the magnetopause moved back and forth, possibly due to reconnection. A strong flow jet with a velocity of $V_L = -400$ km/s was observed, indicating that THE was positioned south of the reconnection X-line. The plasma densities measured by both ESA and spacecraft potential were <10 cm⁻³ inside magnetosphere and >50 cm⁻³ within magnetosheath. After 18:51:40 UT, THE entered the magnetosheath as the magnetic field rotates and plasma densities remain above >50 cm⁻³.

In the dusk sector, THA crossed the magnetopause (beyond geosynchronous orbit) from the magnetosheath side at ~20:06:00 UT and observed weaker flows with $V_L > -200$ km/s (Figure 4i). This crossing reveals an asymmetric magnetopause shape when compared to the magnetopause derived from the Shue model (see Figures 1h and 4m). Inside the magnetosphere, plasma densities inferred from spacecraft potential show values >100 cm⁻³ (Figure 4j) as well as a flux enhancement in the ion energy spectrum below 100 eV (Figure 4h). These observations indicate that a plasmaspheric plume or plasmaspheric material existed on the duskside (e.g., Walsh & Zou, 2021; Walsh, Phan, et al., 2014; Zou et al., 2021). Note that plasma densities obtained from ESA within the magnetosphere decrease to 10 cm⁻³, which contrast with those obtained from the spacecraft potential. This discrepancy can be attributed to the fact that the energy range of cold plasma falls below the energy threshold of ESA (\sim 8 eV). Nonetheless, there were instances of surges in plasma densities exceeding 80 cm⁻³ after 20:11 UT. This surge was a result of the acceleration of the previously occupied cold plasmas due to magnetopause motion (e.g., Sauvaud et al., 2001).

The ion pitch angle distribution within the energy range of 10–100 eV is presented in Figures 4e and 4k. In general, plume particles tend to align predominantly perpendicular to the local magnetic field, whereas warm plasma cloak particles typically align either parallel or anti-parallel (e.g., Lee et al., 2016). Analysis here reveals that the pitch angle distribution was primarily perpendicular to the magnetic field line in the duskside magnetosphere, further supporting that the plume contributed to the measured elevated plasma density. For additional confirmation of the plume's presence, Figure 4m presents GPS TEC measurements mapped from the ionosphere to the equatorial plane of the magnetosphere using the IGRF model (e.g., Walsh, Foster, et al., 2014). Although the mapping is not perfect since the TEC is the total number of electrons integrated along the path between receivers and GPS satellites, the plume measured in the ionosphere aligns well with the local time of the G13 and THA locations. The plume plasmas appear predominantly on the duskside.

The study estimated the in situ reconnection rate from THEMIS observations using the method in Borovsky et al. (2013),

$$R = \frac{\left(\rho_S B_M\right)^{1/2}}{\left(\rho_M B_S + \rho_S B_M\right)^{1/2}}.$$

This method considers the fractional reduction of the local dayside reconnection rate due to a nonzero magnetospheric mass density. Here, ρ is the plasma mass density, B is the reconnecting component of the magnetic field, and M and S denote the magnetosphere and magnetosphere and ρ 0 goes to zero, ρ 1 becomes 1. Thus, ρ 1 is conveniently written as the normalized reconnection rate,

$$R = (1 + MC)^{-1/2}$$

where the ratio

$$MC = \rho_M B_S / \rho_S B_M$$

KIM ET AL. 7 of 11

is the mass-correction factor (or mass inflow ratio). Assuming that the effective mass is similar for the plasma on both sides of the magnetopause (e.g., Walsh, Phan, et al., 2014), the current study estimated the reconnection rates using 15-s averaged magnetic field and plasma density measurements obtained just inside and outside the magnetopause. For THE, the study used plasma density measurements inferred from the spacecraft potential. For THA, the study used plasma density measurement from ESA in the magnetosheath and from spacecraft potential in the magnetosphere, because plasma density inferred from spacecraft potential showed unusual values less than $10~\text{cm}^{-3}$ in the magnetosheath. The estimated reconnection rates were 0.92 (MC = 0.18) for THE and 0.83 (MC = 0.46) for THA. Therefore, the combined observations from SuperDARN and THEMIS suggest that reconnection was more active on the dawnside and presence of cold dense plasma served to reduce the reconnection rate (Walsh & Zou, 2021), resulting in a dawn-dusk asymmetry of the magnetopause erosion at geosynchronous orbit.

To further verify whether magnetopause crossings from THA and THE exhibited reconnection signatures, the study employed the Walén test to assess the consistency of the reconnection jet with predictions derived from tangential stress balance across a rotational discontinuity (Phan et al., 2013; Sonnerup et al., 1981). In this analysis, the study computed a ratio (Δv) between the observed and predicted flow velocities in the time period 18:51:35–18:51:45 UT for THE and 20:06:00–20:06:10 UT for THA. Perfect agreement with theory would result in $\Delta v = 1$, whereas lower Δv would indicate less agreement (Paschmann et al., 1986; Zou et al., 2019). Additionally, the study evaluated the kinetic signature of the reconnection, which manifests as D-shaped ion distributions at the magnetopause, since the plasma entering from the magnetosheath would be present only above a cutoff parallel velocity (Broll et al., 2017; Cowley, 1982; Smith & Rodgers, 1991). In the analysis here, measurements from THE find $\Delta v = 0.7$ while THA finds a $\Delta v = 0.2$ within the magnetopause, while both satellites measured a clearly defined D-shaped ion distribution (Figures 4f and 4i). These results support that both satellites observed reconnection signatures, although there is a lack of agreement in Δv for the THA observation.

4. Discussion and Conclusion

In this letter, we presented the first direct observations of reconnection and its consequential magnetopause erosion at geosynchronous orbit. During the geomagnetic storm main phase, the dawn-dusk asymmetry of magnetopause erosion was observed, with G15 on the dawnside (10.6 MLT) detecting a GMC while G13 on the duskside (14.6 MLT) remained within the magnetosphere. Combined observations from SuperDARN and THEMIS confirmed that reconnection was the primary driver of magnetopause erosion and the asymmetry of erosion was possibly attributed to the different reconnection efficiencies.

The asymmetric magnetopause erosion at geosynchronous orbit can be attributed to the presence of a plasma-spheric drainage plume composed of cold dense plasma. During geomagnetic storms, this plume predominantly occupies the duskside region and can mass-load the dayside reconnection site (Borovsky & Denton, 2008; Su et al., 2000). Modeling studies have shown that the plume reduces the reconnection rate by mass-loading the reconnection site (Borovsky et al., 2008, 2013). Walsh, Phan, et al. (2014) demonstrated experimentally that the velocity of a reconnection jet decreases when the reconnecting magnetopause encounters the plume, indicating less efficient reconnection. A comprehensive study conducted by Zou et al. (2021), which integrates in-situ satellite measurements with ground-based remote sensing, showed that the reconnection rate diminishes by 68%–80% in the presence of the plume compared to regions without it. Observations from the current study have confirmed these findings, revealing a notably weaker reconnection rate in regions influenced by dense plasma-sphere material. Consequently, the study infers that the presence of cold dense plasma on the duskside of the magnetosphere served to reduce the reconnection rate, leading to more efficient magnetopause erosion on the dawnside. Furthermore, this finding also suggests that the predominance of magnetopause erosion on the dawnside, as reported by Dmitriev et al. (2004), may be caused by the plume because the common location where the plume contacts the magnetopause is on the duskside (Walsh et al., 2013).

As the current work has focused on magnetopause erosion in geosynchronous orbit, it is worth noting that the magnetopause is not a perfect sphere, thus asymmetric GMCs can be observed at circular geosynchronous orbits even in the absence of reconnection. A different location of GOES in the Z_{GSM} direction may possibly contribute to asymmetric GMC. Therefore, the geometric approach and the relative location of the satellites, in conjunction with the parabolic shape of the magnetopause, may contribute to the observation of an asymmetric magnetopause.

KIM ET AL. 8 of 11

Acknowledgments

We acknowledge NASA contract NAS5-

02099 and V. Angelopoulos for use of data from the THEMIS Mission. Specifically:

Baumjohann for the use of FGM data, C. W. Carlson and J. P. McFadden for use of

gratefully acknowledge the GOES team for providing the data to the public. The

ESA data, and J. W. Bonnell and F. S. Mozer for use of EFI data. The authors

authors acknowledge the use of

SuperDARN data. SuperDARN is a network of radars funded by national

Canada, China, France, Italy, Japan,

Norway, South Africa, the United Kingdom, and the United States of America. The Kapuskasing SuperDARN radar is maintained and operated by

and operated by the University of

Saskatchewan. We also appreciate the availability of GPS TEC data. GPS TEC

data products and access through the Madrigal distributed data system are

provided to the community by the

Massachusetts Institute of Technology

Foundation Grant AGS-1242204. We

thank the THEMIS SPEDAS team for

under support from US National Science

providing their open-source library of data

analysis tools (Angelopoulos et al., 2019).

N27]. For the purpose of Open-Access, the

copyright license to any author accepted manuscript version arising from this

submission. HC gratefully acknowledges support from the NASA GSFC ISFM

Space Precipitation Impacts program, the NSF Grant AGS-1928883, and the NASA

80NSSC20K1670, and 80MSFC20C0019.

FP is supported by the Federal Ministry for

Economic Affairs and Climate Action (BMWK) and the German Aerospace

Center under contract 50 OC 2201.

Grants, 80NSSC19K0844,

author has applied a CC BY public

This research was funded in part by the Austrian Science Fund (FWF) [P32175-

scientific funding agencies of Australia,

Virginia Tech under support by NSF Grant AGS-1935110. The Saskatoon and Prince

George SuperDARN radars are maintained

K. H. Glassmeier, U. Auster, and W.

Asymmetric solar wind pressure or fronts can also lead to uneven magnetopause compression because the magnetopause motion into geosynchronous orbit should be accompanied by strong solar wind pressure. If a solar wind front approaches at an angle, such as with a strong east-west component of IMF (B_y) , one would also anticipate asymmetric compression of the magnetopause (e.g., Oliveira & Raeder, 2014). Furthermore, dayside transients, such as hot-flow anomalies, foreshock bubbles, and magnetosheath jets, can be responsible for the asymmetric magnetopause shape (e.g., Fairfield et al., 1990; Grimmich et al., 2023; Zhang et al., 2022). Additionally, aside from reconnection, other mechanisms such as the ring current and region-1 field-aligned current can contribute to the creation of asymmetric magnetopause erosion by reducing the magnetic field strength within the dayside magnetosphere (Sibeck, 1994; Tsyganenko & Sibeck, 1994). Therefore, erosion of the magnetopause and its asymmetry in the geosynchronous orbit are active, but other elements may also play a role.

Although we showed valuable SuperDARN observations as evidence of reconnection, further investigations with a larger number of GMCs are necessary to precisely quantify the extent of reconnection's contribution to magnetopause erosion at geosynchronous orbit. It is still challenging to locate concurrent observations of erosion and reconnection due to the masking of radar echoes by high plasma density in the dayside, mid-latitude ionosphere during high solar activity (Koustov et al., 2022). Fortunately, the upcoming launches of the Lunar Environment Heliospheric X-ray Imager (LEXI; Walsh et al., 2020) and the Solar wind-Magnetosphere-Ionosphere Link Explorer (SMILE; Branduardi-Raymont et al., 2018) in 2024 and 2025, respectively, will provide a global perspective of the magnetopause through soft X-ray images. These missions will provide consecutive magnetopause images, promising to enhance our comprehensive understanding of the magnetopause configuration and its intricate relationship with reconnection processes.

Data Availability Statement

We accessed THEMIS data from http://themis.ssl.berkeley.edu/data/themis/ and used Level 2 data for FGM and ESA. GOES magnetic field data can be found at https://www.ngdc.noaa.gov/stp/satellite/goes/dataaccess.html. SuperDARN data are accessible at Kim (2024). TEC data are available at http://cedar.openmadrigal.org/single? isGlobal=on&categories=17&instruments=8000&years=2014&months=2&days=27 with registration. The solar wind data are available through NASA OMNI web database at https://omniweb.gsfc.nasa.gov.

References

Angelopoulos, V. (2008). The THEMIS mission. Space Science Reviews, 141(1-4), 5-34. https://doi.org/10.1007/s11214-008-9336-1

Angelopoulos, V., Cruce, P., Drozdov, A., Grimes, E. W., Hatzigeorgiu, N., King, D. A., et al. (2019). The space physics environment data analysis system (SPEDAS). Space Science Reviews, 215(1), 9. https://doi.org/10.1007/s11214-018-0576-4

Auster, H. U., Glassmeier, K. H., Magnes, W., Aydogar, O., Baumjohann, W., Constantinescu, D., et al. (2008). The THEMIS fluxgate magnetometer. Space Science Reviews, 141(1-4), 235-264. https://doi.org/10.1007/s11214-008-9365-9

Bonnell, J. W., Mozer, F. S., Delory, G. T., Hull, A. J., Ergun, R. E., Cully, C. M., et al. (2008). The electric field instrument (EFI) for THEMIS. Space Science Reviews, 141, 303–341. https://doi.org/10.1007/s11214-008-9469-2

Borovsky, J. E., & Denton, M. H. (2008). A statistical look at plasmaspheric drainage plumes. *Journal of Geophysical Research*, 113(A9), A09221. https://doi.org/10.1029/2007JA012994

Borovsky, J. E., Denton, M. H., Denton, R. E., Jordanova, V. K., & Krall, J. (2013). Estimating the effects of ionospheric plasma on solar wind/magnetosphere coupling via mass loading of dayside reconnection: Ion-plasma-sheet oxygen, plasmaspheric drainage plumes, and the plasma cloak. *Journal of Geophysical Research: Space Physics*, 118(9), 5695–5719. https://doi.org/10.1002/jgra.50527

Borovsky, J. E., Hesse, M., Birn, J., & Kuznetsova, M. M. (2008). What determines the reconnection rate at the dayside magnetosphere? *Journal of Geophysical Research*, 113(A7), A07S12. https://doi.org/10.1029/2007ja012645

Branduardi-Raymont, G., Wang, C., Dai, L., Donovan, E., Li, L., Sembay, S., et al. (2018). SMILE Definition study report (red book). ESA/SCI (2018)1. Retrieved from https://sci.esa.int/web/smile/-/61194-smile-definition-study-report-red-book

Broll, J. M., Fuselier, S. A., & Trattner, K. J. (2017). Locating dayside magnetopause reconnection with exhaust ion distributions. *Journal of Geophysical Research: Space Physics*, 122, 5105–5113. https://doi.org/10.1002/2016JA023590

Chapman, S., & Ferraro, V. C. A. (1931). A new theory of magnetic storms. *Terrestrial Magnetism and Atmospheric Electricity*, 36(3), 171–186. https://doi.org/10.1029/TE036i003p00171

Chen, X.-C., Lorentzen, D. A., Moen, J. I., Oksavik, K., Baddeley, L. J., & Lester, M. (2016). Fregion ionosphere effects on the mapping accuracy of SuperDARN HF radar echoes. *Radio Science*, 51(5), 490–506. https://doi.org/10.1002/2016RS005957

Chisham, G., & Freeman, M. P. (2003). A technique for accurately determining the cusp-region polar cap boundary using SuperDARN HF radar measurements. Annals of Geophysics, 21(4), 983–996. https://doi.org/10.5194/angeo-21-983-2003

Chisham, G., Freeman, M. P., Abel, G. A., Lam, M. M., Pinnock, M., Coleman, I. J., et al. (2008). Remote sensing of the spatial and temporal structure of magnetopause and magnetotail reconnection from the ionosphere. *Reviews of Geophysics*, 46(1), RG1004. https://doi.org/10.1029/2007PG000233

Chisham, G., Lester, M., Milan, S. E., Freeman, M. P., Bristow, W. A., Grocott, A., et al. (2007). A decade of the super dual Auroral radar network (SuperDARN): Scientific achievements, new techniques and future directions. Surveys in Geophysics, 28(1), 33–109. https://doi.org/10.1007/s10712-007-9017-8

KIM ET AL. 9 of 11

- Cowley, S. W. H. (1982). The causes of convection in the Earth's magnetosphere: A review of developments during the IMS. Reviews of Geophysics and Space Physics, 20(3), 531–565. https://doi.org/10.1029/rg020i003p00531
- Cowley, S. W. H., & Lockwood, M. (1992). Excitation and decay of solar wind-driven flows in the magnetosphere-ionosphere system. Annales Geophysicae, 10, 103–115.
- Dmitriev, A. V., Suvorova, A. V., Chao, J. K., & Yang, Y.-H. (2004). Dawn-dusk asymmetry of geosynchronous magnetopause crossings. Journal of Geophysical Research, 109(A5), A05203. https://doi.org/10.1029/2003JA010171
- Fairfield, D. H. (1971). Average and unusual locations of the Earth's magnetopause and bow shock. *Journal of Geophysical Research*, 76(28), 6700–6716. https://doi.org/10.1029/JA076i028p06700
- Fairfield, D. H., Baumjohann, W., Paschmann, G., Luhr, H., & Sibeck, D. G. (1990). Upstream pressure variations associated with the bow shock and their effects on the magnetosphere. *Journal of Geophysical Research*, 95, 3773.
- Greenwald, R. A., Baker, K. B., Dudeney, J. R., Pinnock, M., Jones, T. B., Thomas, E. C., et al. (1995). DARN/SuperDARN. Space Science Reviews, 71(1–4), 761–796. https://doi.org/10.1007/BF00751350
- Grimmich, N., Plaschke, F., Archer, M. O., Heyner, D., Mieth, J. Z. D., Nakamura, R., & Sibeck, D. G. (2023). Study of extreme magnetopause distortions under varying solar wind conditions. *Journal of Geophysical Research: Space Physics*, 128(8), e2023JA031603. https://doi.org/10. 1029/2023JA031603
- Hubert, B., Milan, S. E., Grocott, A., Blockx, C., Cowley, S. W. H., & Gerard, J.-C. (2006). Dayside and nightside reconnection rates inferred from IMAGE FUV and Super Dual Auroral Radar Network data. *Journal of Geophysical Research*, 111(A3), A03217. https://doi.org/10.1029/ 2005JA011140
- Kim, H. (2024). SuperDARN data used in the study of localized magnetopause erosion at geosynchronous orbit by reconnection [Dataset]. Zenodo, 462. https://doi.org/10.5281/zenodo.10450956
- Koustov, A. B., Ullrich, S., Ponomarenko, P. V., Ghalamkarian Nejad, M., Themens, D. R., & Gillies, R. G. (2022). Occurrence rates of SuperDARN ground scatter echoes and electron density in the ionosphere. *Radio Science*, 57, 11. https://doi.org/10.1029/2022RS007520
- Le, G., Lühr, H., Anderson, B. J., Strangeway, R. J., Russell, C. T., Singer, H., et al. (2016). Magnetopause erosion during the 17 March 2015 magnetic storm: Combined field-aligned currents, auroral oval, and magnetopause observations. Geophysical Research Letters, 43(6), 2396–2404. https://doi.org/10.1002/2016GL068257
- Lee, S. H., Zhang, H., Zong, Q.-G., Otto, A., Rème, H., & Liebert, E. (2016). A statistical study of plasmaspheric plumes and ionospheric outflows observed at the dayside magnetopause. *Journal of Geophysical Research: Space Physics*, 121(1), 492–506. https://doi.org/10.1002/ 2015JA021540
- Maezawa, K. (1974). Dependence of the magnetopause position on the southward interplanetary magnetic field. Planetary and Space Science, 22(10), 1443–1453. https://doi.org/10.1016/0032-0633(74)90040-3
- McComas, D. J., Bame, S. J., Barraclough, B. L., Donart, J. R., Elphic, R. C., Gosling, J. T., et al. (1993). Magnetospheric plasma analyzer (MPA): Initial three-spacecraft observations from geosynchronous orbit. *Journal of Geophysical Research*, 98(13), 453.
- McComas, D. J., Elphic, R. C., Moldwin, M. B., & Thomsen, M. F. (1994). Plasma observations of magnetopause crossings at geosynchronous orbit. *Journal of Geophysical Research*, 99(21), 249–21255. https://doi.org/10.1029/94ja01094
- McFadden, J. P., Carlson, C. W., Larson, D., Ludlam, M., Abiad, R., Elliott, B., et al. (2008). The THEMIS ESA plasma instrument and in-flight calibration. Space Science Reviews, 141(1–4), 277–302. https://doi.org/10.1007/s11214-008-9440-2
- Nishitani, N., Ruohoniemi, J. M., Lester, M., Baker, J. B. H., Koustov, A. V., Shepherd, S. G., et al. (2019). Review of the accomplishments of mid-latitude super dual auroral radar network (SuperDARN) HF radars. Progress in Earth and Planetary Science, 6(1), 27. https://doi.org/10.1186/s40645-019-0270-5
- Oliveira, D. M., & Raeder, J. (2014). Impact angle control of interplane-tary shock geoeffectiveness. *Journal of Geophysical Research: Space Physics*, 119(10), 8188–8201. https://doi.org/10.1002/2014JA020275
- Paschmann, G., Papamastorakis, I., Baumjohann, W., Sckopke, N., Carlson, C. W., Sonnerup, B. U. Ö., & Lühr, H. (1986). The magnetopause for large magnetic shear: AMPTE/IRM observations. *Journal of Geophysical Research*, 91(A10), 11099–11115. https://doi.org/10.1029/ja091ia10p11099
- Petrinec, S. P., Song, P., & Russell, C. T. (1991). Solar cycle variations in the size and shape of the magnetopause. *Journal of Geophysical Research*, 96(A5), 7893–7896. https://doi.org/10.1029/90ja02566
- Phan, T. D., Paschmann, G., Gosling, J. T., Oieroset, M., Fujimoto, M., Drake, J. F., & Angelopoulos, V. (2013). The dependence of magnetic reconnection on plasma β and magnetic shear: Evidence from magnetopause observations. *Geophysical Research Letters*, 40(1), 11–16. https://doi.org/10.1029/2012GL054528
- Rufenach, C. L., Martin, R. F., Jr., & Sauer, H. H. (1989). A study of geosynchronous magnetopause crossings. *Journal of Geophysical Research*, 94(15), 125–15134. https://doi.org/10.1029/ja094ia11p15125
- Ruohoniemi, J. M., & Baker, K. B. (1998). Large-scale imaging of highlatitude convection with super dual auroral radar network HF radar observations. *Journal of Geophysical Research*, 103(A9), 20797–20811. https://doi.org/10.1029/98JA01288
- Russell, C. T. (1976). On the occurrence of magnetopause crossings at 6.6 RE. Geophysical Research Letter, 3(593), 593–595. https://doi.org/10.1029/gl003i010p00593
- Sauvaud, J.-A., Lundin, R., Rème, H., McFadden, J. P., Carlson, C., Parks, G. K., et al. (2001). Intermittent thermal plasma acceleration linked to sporadic motions of the magnetopause, first Cluster results. *Annals of Geophysics*, 19(10/12), 1523–1532. https://doi.org/10.5194/angeo-19-1523-2001
- Shepherd, S. G. (2014). Altitude-adjusted corrected geomagnetic coordinates: Definition and functional approximations. *Journal of Geophysical Research*, 119(7), 7501–7521. https://doi.org/10.1002/2014JA020264
- Shue, J.-H., Song, P., Russell, C. T., Steinberg, J. T., Chao, J. K., Zastenker, G., et al. (1998). Magnetopause location under extreme solar wind conditions. *Journal of Geophysical Research*, 103(A8), 17691–17700. https://doi.org/10.1029/98JA01103
- Sibeck, D. G. (1994). Signatures of flux erosion from the dayside magnetosphere. Journal of Geophysical Research, 99(A5), 8513–8529. https://doi.org/10.1029/931A03298
- Smith, M., & Rodgers, D. (1991). Ion distributions at the dayside magnetopause. *Journal of Geophysical Research*, 96(A7), 11617–11624. https://doi.org/10.1029/91ja00676
- Sonnerup, B. U. Ö., & Cahill, L. J., Jr. (1967). Magnetopause structure and attitude from explorer 12 observations. *Journal of Geophysical Research*, 72(1), 171–183. https://doi.org/10.1029/JZ072i001p00171
- Sonnerup, B. U. Ö., Paschmann, G., Papamastorakis, I., Sckopke, N., Haerendel, G., Bame, S. J., et al. (1981). Evidence for magnetic field reconnection at the earth's magnetopause. *Journal of Geophysical Research*, 86(A12), 10049–10067. https://doi.org/10.1029/

KIM ET AL. 10 of 11

- Su, Y.-J., Borovsky, J. E., Thomsen, M. F., Elphic, R. C., & McComas, D. J. (2000). Plasmaspheric material at the reconnecting magnetopause. Journal of Geophysical Research, 105, 7591–7600. https://doi.org/10.1029/1999JA000266
- Trattner, K. J., Petrinec, S. M., & Fuselier, S. A. (2021). The location of magnetic reconnection at earth's magnetopause. *Space Science Reviews*, 217(3), 41. https://doi.org/10.1007/s11214-021-00817-8
- Tsyganenko, N. A. (1989). A magnetospheric magnetic field model with a warped tail current sheet. *Planetary and Space Science*, 37(1), 5–20. https://doi.org/10.1016/0032-0633(89)90066-4
- Tsyganenko, N. A., & Sibeck, D. J. (1994). Concerning flux erosion from the dayside magnetosphere. *Journal of Geophysical Research*, 99(A7), 13425–13436. https://doi.org/10.1029/94ja00719
- Tsyganenko, N. A., & Sitnov, M. I. (2005). Modeling the dynamics of the inner magnetosphere during strong geomagnetic storms. *Journal of Geophysical Research*, 110(A3), A03208. https://doi.org/10.1029/2004JA010798
- Walsh, B. M., Collier, M., Busk, S., Connor, H., Kuntz, K., McShane, J., et al. (2020). The Lunar Environment Heliospheric X-ray imager (LEXI)

 —A mission for global magnetospheric imaging. In AGU fall meeting 2020 SM029-01.
- Walsh, B. M., Foster, J. C., Erickson, P. J., & Sibeck, D. G. (2014). Simultaneous ground- and space-based observations of the plasmaspheric plume and reconnection. *Science*, 343(6175), 1122–1125. https://doi.org/10.1126/science.1247212
- Walsh, B. M., Phan, T. D., Sibeck, D. G., & Souza, V. M. (2014). The plasmaspheric plume and magnetopause reconnection. *Geophysical Research Letters*, 41(2), 223–228. https://doi.org/10.1002/2013gl058802
- Walsh, B. M., Sibeck, D. G., Nishimura, Y., & Angelopoulos, V. (2013). Statistical analysis of the plasmaspheric plume at the magnetopause. Journal of Geophysical Research: Space Physics, 118(8), 4844–4851. https://doi.org/10.1002/jgra.50458
- Walsh, B. M., & Zou, Y. (2021). The role of magnetospheric plasma in solar wind-magnetosphere coupling: A review. *Journal of Atmospheric and Solar-Terrestrial Physics*, 219, 105644. https://doi.org/10.1016/j.jastp.2021.105644
- Wrenn, G. L., Johnson, J. F. E., Norris, A. J., & Smith, M. F. (1981). GEOS-2 magnetopause encounters: Low energy (<500 eV) particle measurements. *Advances in Space Research*, 1, 129–134. https://doi.org/10.1016/0273-1177(81)90096-x
- Zhang, H., Zong, Q., Connor, H., Delamere, P., Facskó, G., Han, D., et al. (2022). Dayside transient phenomena and their impact on the magnetosphere and ionosphere. Space Science Reviews, 218(5), 40. https://doi.org/10.1007/s11214-021-00865-0
- Zou, Y., Walsh, B. M., Chen, L.-J., Ng, J., Shi, X., Wang, C.-P., et al. (2022). Unsteady magnetopause reconnection under quasi-steady solar wind driving. *Geophysical Research Letters*, 49(1), e2021GL096583. https://doi.org/10.1029/2021GL096583
- Zou, Y., Walsh, B. M., Nishimura, Y., Angelopoulos, V., Ruohoniemi, J. M., McWilliams, K. A., & Nishitani, N. (2019). Local time extent of magnetopause reconnection using space–ground coordination. *Annals of Geophysics*, 37(2), 215–234. https://doi.org/10.5194/angeo-37-215-2010
- Zou, Y., Walsh, B. M., Shi, X., Lyons, L., Liu, J., Angelopoulos, V., et al. (2021). Geospace plume and its impact on dayside magnetopause reconnection rate. *Journal of Geophysical Research: Space Physics*, 126(6), e2021JA029117. https://doi.org/10.1029/2021JA029117

KIM ET AL. 11 of 11